

## Article

# Be Careful What You Wish for: Cost Function Sensitivity in Predictive Simulations for Assistive Device Design

Ali Nikoo and Thomas K. Uchida \*

Department of Mechanical Engineering, University of Ottawa, 161 Louis-Pasteur, Ottawa, ON K1N 6N5, Canada  
\* Correspondence: tuchida@uottawa.ca; Tel.: +1-613-562-5800

**Abstract:** Software packages that use optimization to predict the motion of dynamic systems are powerful tools for studying human movement. These “predictive simulations” are gaining popularity in parameter optimization studies for designing assistive devices such as exoskeletons. The cost function is a critical component of the optimization problem and can dramatically affect the solution. Many cost functions have been proposed that are biologically inspired and that produce reasonable solutions, but which may lead to different conclusions in some contexts. We used OpenSim Moco to generate predictive simulations of human walking using several cost functions, each of which produced a reasonable trajectory of the human model. We then augmented the model with motors that generated hip flexion, knee flexion, or ankle plantarflexion torques, and repeated the predictive simulations to determine the optimal motor torques. The model was assumed to be planar and bilaterally symmetric to reduce computation time. Peak torques varied from 41.3 to 79.0 N·m for the hip flexion motors, from 48.0 to 94.2 N·m for the knee flexion motors, and from 42.6 to 79.8 N·m for the ankle plantarflexion motors, which could have important design consequences. This study highlights the importance of evaluating the robustness of results from predictive simulations.



**Citation:** Nikoo, A.; Uchida, T.K. Be Careful What You Wish for: Cost Function Sensitivity in Predictive Simulations for Assistive Device Design. *Symmetry* **2022**, *14*, 2534. <https://doi.org/10.3390/sym14122534>

Academic Editor: Jan Awrejcewicz

Received: 20 October 2022

Accepted: 22 November 2022

Published: 30 November 2022

**Publisher’s Note:** MDPI stays neutral with regard to jurisdictional claims in published maps and institutional affiliations.



**Copyright:** © 2022 by the authors. Licensee MDPI, Basel, Switzerland. This article is an open access article distributed under the terms and conditions of the Creative Commons Attribution (CC BY) license (<https://creativecommons.org/licenses/by/4.0/>).

## 1. Introduction

Musculoskeletal modeling and simulation are powerful tools for studying the biomechanics of human movement. Simulations can complement the knowledge gained from experiments by providing estimates of variables that are difficult or impossible to measure directly. For example, experimental studies have directly measured the whole-body metabolic energy expended during steady-state walking over a range of speeds [1], but simulations are required to examine how metabolic energy consumption is distributed between the phases of gait [2] and throughout the body [3]. Simulations also enable one to study the effect of changes in parameters that cannot easily be isolated or adjusted experimentally, such as the effect of tendon compliance on metabolic energy expenditure during running [4]. Finally, simulations can reveal fundamental principles that govern movement, such as the neural control strategies involved in reaching [5], maintaining balance [6], and locomotion [7].

Many studies gain deeper insight into measurements of human movement by generating inverse kinematic and inverse dynamic simulations from experimental data [8]. For example, Arnold et al. [9] generated simulations from experimental data to estimate the lengths and velocities of muscle fibers during walking, thereby revealing how the force-generation capacity of our muscles varies over the gait cycle. An emerging application of musculoskeletal models and the simulation of movement is in the design optimization of wearable assistive devices such as exoskeletons and soft exosuits, which apply forces to the body to make movement safer or more economical. For example, inverse dynamic simulations were used to understand how assistive devices can be designed to reduce the metabolic energy consumed during running [10] and during walking while carrying a

heavy load [3]. These simulations suggested that assistive devices should not merely aim to mimic net biological joint moments during unassisted movement: such a design strategy would generally fail to minimize metabolic energy expenditure as it would ignore, among other things, the necessary activity of muscles that span both assisted and unassisted joints. The simulation results of Uchida et al. [10] were experimentally validated by Lee et al. [11], who used the simulations to tune the actuation profile for their soft exosuit, one of the first assistive devices to reduce the metabolic energy consumed during running. Despite the utility of inverse dynamic simulations, they are fundamentally limited because they track experimental data and, therefore, they assume that the joint kinematics and ground reaction forces do not change when an assistive device is worn. Some studies have suggested that assistive devices may not change joint kinematics substantially [12,13] or that kinematics may change initially but will ultimately return to normal following an adaptation period [14]. However, many studies have reported large, persisting differences in kinematics between assisted and unassisted gait [15–17].

The limitations of inverse dynamic analyses can be addressed using simulations that predict human movement without tracking experimental data [18,19]. These “predictive simulations” use numerical optimization to determine the actuation signals (e.g., net joint torques or the excitations of individual muscles) that must be applied to a model of the musculoskeletal system in order to achieve the best possible performance at a defined task. The quantities that must be determined are called design variables and may include parameters of the musculoskeletal model, parameters of an assistive device, gains of neuromuscular or device controllers, actuation signals, applied forces, initial conditions, or other quantities. The desired task is encoded into a cost function (or objective function), a mathematical function of the design variables that describes the nature of the solution being sought. An optimizer determines a set of values for the design variables that minimizes the cost function, while also satisfying one or more constraint equations. The constraint equations describe any equalities or inequalities that must be satisfied for the solution to be considered valid, such as obeying Newton’s laws of motion and respecting bounds on the design variables. If the cost function has been judiciously designed, the desired movement (e.g., a human-like walking gait at a desired speed) will emerge as the solution to the optimization problem.

Predictive simulations enable one to study scenarios that would be time-consuming or otherwise onerous to explore using experiments. For example, hypothetical designs for prostheses can be evaluated and optimized without constructing physical prototypes, recruiting study participants, or conducting data collection sessions in the lab [20,21]. Predictive simulations do not track experimental data and, therefore, they do not assume that the joint kinematics and ground reaction forces remain unchanged during device-assisted gait; however, the solution that is found depends on the cost function that is specified. Defining the cost function may be straightforward in some applications—for example, in an optimal control problem where a robot must jump as high as possible. Unfortunately, the cost functions governing human movement are not known precisely. It is known that humans tend to prefer walking in metabolically economical ways [22]; hence, metabolic energy expenditure (specifically, the cost of transport or the energy consumed per distance traveled) often appears as a term in the cost function for predictive simulations of gait [2,18–20,23–30]. Other commonly used terms include the minimization of muscle effort or work [24,26,28,30–37], fatigue [35,36,38], ligament strain [29,30], joint torque [28,39], joint load [25], head motion [19,29,30], asymmetry [34,35], and the derivative of ground reaction force [30,33]—each of which can be justified biologically. Many combinations and relative weightings of these cost function terms have been used in the literature to generate predictive simulations of gait with realistic joint kinematics and other features. However, when predictive simulations are used to optimize the design of assistive devices, it is unknown whether the resulting designs are sensitive to the selected cost function.

In this study, we explore the robustness of assistive devices that have been designed using predictive simulations. The simulations are generated in OpenSim Moco using a planar, bilaterally symmetric musculoskeletal model with 18 muscles. OpenSim Moco

provides users with an interface for posing optimal control problems and employs the direct collocation method to improve the computational efficiency of solving them. OpenSim Moco has been used to generate predictive simulations of a variety of human movements, including healthy and atypical walking [40], squat-to-stand [40], cycling [41], single-leg landing [42], running [43], and reaching [44]. We first generate predictive simulations of walking using six plausible cost functions, each of which produces a realistic gait pattern. We then augment the musculoskeletal model with motors that generate hip flexion, knee flexion, or ankle plantarflexion torques, where the torques generated by the assistive devices are optimized along with the muscle forces and motion of the model. We demonstrate that, although many cost functions produce similar joint kinematics during gait, they may result in dramatically different conclusions about the design of an assistive device. This study highlights the importance of evaluating the sensitivity of predictive simulations to the cost function that is specified.

## 2. Methodology

All simulations were performed in OpenSim Moco [40] version 1.1.0. The simulation workflow comprised three steps:

1. Find an initial guess for the predictive simulations. An optimization problem was solved to track measured joint kinematics and ground reaction forces with a musculoskeletal model.
2. Generate predictive simulations of unassisted gait. Simulations were generated using six cost functions, using the solution from step 1 as the initial guess for each optimization problem.
3. Generate predictive simulations of assisted gait. Assistive devices were added to the model bilaterally at the hip, knee, or ankle. Simulations were generated using the same six cost functions as in step 2, again using the solution from step 1 as the initial guess for each optimization problem.

These steps are described in detail below.

### 2.1. Musculoskeletal Model

We used the “2D\_gait.osim” model, shown in Figure 1, which is a modified version of the “gait10dof18musc.osim” model and is provided with OpenSim [45,46]. The model is planar, bilaterally symmetric, has a mass of 62.0 kg, and has 10 degrees of freedom: the tilt, horizontal displacement, and vertical displacement of the pelvis relative to the fixed ground frame; the angle of the lumbar joint between the pelvis and the rigid upper body; and hip flexion/extension, knee flexion/extension, and ankle plantarflexion/dorsiflexion on each leg. The musculoskeletal model is actuated by nine muscles on each leg, representing the main muscles (or muscle groups) that are responsible for producing gait in the sagittal plane: gluteus maximus, biarticular hamstrings, biceps femoris short head, gastrocnemius, soleus, iliopsoas, rectus femoris, vasti, and tibialis anterior. Muscle forces are computed using the “DeGrooteFregly2016Muscle” Hill-type model [47]. An ideal motor at the lumbar joint is used to represent the combined activity of the torso muscles. The foot–ground interaction was modeled by two spheres on each foot using the “SmoothSphereHalfSpace-Force” model [48], which is a differentiable approximation of the Hunt–Crossley contact model [49]. All parameters were identical to those provided in the “2D\_gait.osim” model except for the stiffness of the contact spheres, which was set to  $k = 9.4281 \times 10^5 \text{ N/m}^2$  following the work of Dorn et al. [19].

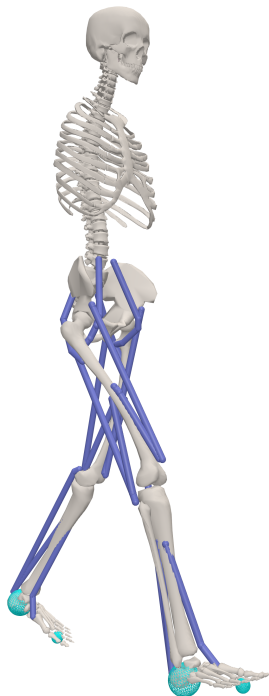


**Figure 1.** Planar, bilaterally symmetric musculoskeletal model used to generate predictive simulations in OpenSim Moco.

## 2.2. Initial Guess for Predictive Simulations

Predictive simulations are generated by solving optimization problems, which require initial guesses. Due to the complexity of the optimization problems that are solved in predictive simulations of gait, it is critical to use a good initial guess; otherwise, the optimization problem can require an unreasonable amount of computational effort. In this work, an initial optimization problem was solved to track measured joint kinematics and ground reaction forces. Specifically, the MocoTrack tool in OpenSim Moco was used to determine the forces that must be applied by the actuators (i.e., the 18 muscles and the lumbar joint motor) to drive the musculoskeletal model through a similar trajectory and with similar ground reaction forces as experimental observations. The experimental data were obtained from the work of Falisse et al. [35] and were low-pass filtered at 6 Hz.

The optimization problem was solved eight times using different cost functions, each of which comprised several weighted components (called “goals” in OpenSim Moco). The MocoTrack tool minimized the error between the provided kinematic data and the corresponding variables (states) in the model. A MocoPeriodicityGoal was used to enforce kinematic symmetry between the left and right sides of the body, and to ensure the resulting gait was periodic. The periodicity goal permitted the simulation of only half of a gait cycle (i.e., from right-leg heel strike to left-leg heel strike), which reduced computation time; a complete gait cycle was then assembled by duplicating the joint trajectories from the first half of the gait cycle to the second half, and reflecting them from one leg to the other. A MocoAverageSpeedGoal was used to enforce an average walking speed of 1.33 m/s, which was selected to match the experimental data [35]. A MocoContactTrackingGoal was used to minimize the error between the measured and simulated ground reaction forces in the vertical and horizontal (fore-aft) directions. A MocoControlGoal was used to minimize the sum of squared control signals (muscle excitations and lumbar motor actuation) [50]. A MocoOutputGoal was used to minimize the metabolic energy consumed by the muscles using a smoothed version of the model of Bhargava et al. [51], normalized by the mass of the model and the distance traveled. Finally, a second MocoOutputGoal was defined to minimize the acceleration of the head.

The MocoCasADiSolver was used to solve the tracking problem. The convergence and constraint tolerances were set to  $5 \times 10^{-4}$  based on the results of a convergence

analysis (the default values of  $1 \times 10^{-3}$  were insufficient); default values were used for all other solver settings. The tracking problem was solved eight times to explore the effect of adjusting the relative weighting of the terms in the cost function. To facilitate this analysis, each cost function term was first multiplied by a normalization factor equal to the reciprocal of a representative quantity, thereby normalizing each term to have a value of approximately 1. Thus, the weights reflected the percentage importance ascribed to each term. The normalization factors and weights for the tracking problem cost functions ( $T_1$  to  $T_8$ ) are provided in Table 1; all tracking problems were identical except for the weights of the terms in the cost function. Combinations of weights were selected manually to explore the range of cost functions that would plausibly be used in studies of this nature. Once all tracking simulations had been generated, a single solution was selected and used as the initial guess for all predictive simulations generated in this work.

**Table 1.** Cost functions used in the tracking problem to find an initial guess for the predictive simulations. All cost functions included the state-tracking, periodicity, and average speed goals. (GRF = ground reaction force.)

Cost Function	Weight (Normalization Factor)				
	State Tracking (0.066756)	GRF Tracking (0.019305)	Control Effort (0.507614)	Metabolic Energy (0.256410)	Head Acceleration (0.555556)
$T_1$	0.1	0.1	0.1	0	0.7
$T_2$	0.1	0.3	0.1	0	0.5
$T_3$	0.1	0.5	0.1	0	0.3
$T_4$	0.1	0.7	0.1	0	0.1
$T_5$	0.1	0.1	0.2	0.5	0.1
$T_6$	0.1	0.1	0.2	0.3	0.3
$T_7$	0.1	0.1	0.2	0.1	0.5
$T_8$	0.1	0.3	0.2	0.3	0.1

### 2.3. Predictive Simulations of Unassisted Gait

Predictive simulations were generated using the musculoskeletal model described above (Section 2.1). The optimization problem was solved six times using different cost functions, each of which again comprised several weighted components. A MocoJointReactionGoal was used to minimize the compressive load in each knee—specifically, to minimize the squared component of the knee joint reaction force vector that was perpendicular to the tibial plateau, normalized by the weight of the model. A MocoControlGoal was used to minimize the sum of cubed control signals (muscle excitations and lumbar motor actuation) [52]. The periodicity, average speed, metabolic cost, and head acceleration goals described above (Section 2.2) were also used. Note that experimental data were used only to generate the initial guess for use in the predictive simulations; no experimental data were tracked when generating the predictive simulations. The normalization factors and cost function weights for generating the predictive simulations ( $P_1$  to  $P_6$ ) are provided in Table 2; all optimization problems were identical except for the weights of the terms in the cost function. Combinations of weights were once again selected manually to explore the range of cost functions that would plausibly be used to generate predictive simulations of walking. The MocoCasADiSolver was used to generate all predictive simulations. Convergence and constraint tolerances were again set to  $5 \times 10^{-4}$ , and default values were used for all other solver settings.

**Table 2.** Cost functions used to generate predictive simulations. All cost functions included the periodicity and average speed goals.

Cost Function	Weight (Normalization Factor)			
	Control Effort (0.507614)	Metabolic Energy (0.256410)	Head Acceleration (0.555556)	Knee Load (0.002525)
$P_1$	0.5	0	0.5	0
$P_2$	0	0.3	0.7	0
$P_3$	0.7	0	0.3	0
$P_4$	0.1	0.1	0.8	0
$P_5$	0.2	0.2	0.6	0
$P_6$	0.1	0	0.6	0.3

#### 2.4. Predictive Simulations of Device-Assisted Gait

Assistive devices were added to the model bilaterally at the hip, knee, or ankle. The devices were modeled as motors that applied flexion torques to the hip joints, flexion torques to the knee joints, or plantarflexion torques to the ankle joints. The “optimal force” property was set to 100 N·m in all cases, where a control signal of 0.5, for example, would produce an applied torque of 50 N·m. Predictive simulations were generated using the same cost functions as in the unassisted predictive simulations (i.e.,  $P_1$  to  $P_6$ ) and using the same initial guess in all cases. The torques generated by the assistive devices were parameterized as piecewise linear functions over time, and were optimized along with the muscle forces and motion of the model.

#### 2.5. Results Comparison

The tracking simulation results were evaluated by comparing joint kinematics (hip, knee, and ankle angles) and ground reaction forces (vertical and horizontal components) over one gait cycle to data measured from a population of healthy adults walking at a similar speed [35]. Muscle activations were compared to electromyography (EMG) signals collected during healthy walking [19]. Differences in joint kinematics, ground reaction forces, and muscle activations among the eight tracking simulations (i.e., using each cost function  $T_1$  to  $T_8$ ) were also evaluated. The unassisted predictive simulation results were evaluated by comparing the joint kinematics and ground reaction forces to the same measurements of healthy gait. The cost of transport was also computed for all solutions (i.e., using each cost function  $P_1$  to  $P_6$ ). The device-assisted predictive simulations were evaluated by comparing joint kinematics, ground reaction forces, cost of transport, and peak assistive device torques and powers among all solutions for each assistance strategy. Joint kinematics, ground reaction forces, and assistive device torques and powers were analyzed only for the right leg since the model was symmetric.

### 3. Results

The joint kinematics, ground reaction forces, and muscle activations for the tracking simulations are shown in Figures 2 and 3. As shown in Figures 2 and 3, the tracking simulations capture many salient characteristics of healthy gait. Some differences can be observed between the tracking simulation results and the measured data; however, some differences are expected since the model differs from the physical system in many respects. Most importantly, we note that the joint kinematics, ground reaction forces, and muscle activations are very similar across all tracking simulations, despite having been generated using different cost functions. The value of each cost function at the obtained solution is provided in Table 3. The solution obtained using cost function  $T_4$  was selected for use as the initial guess for all predictive simulations.

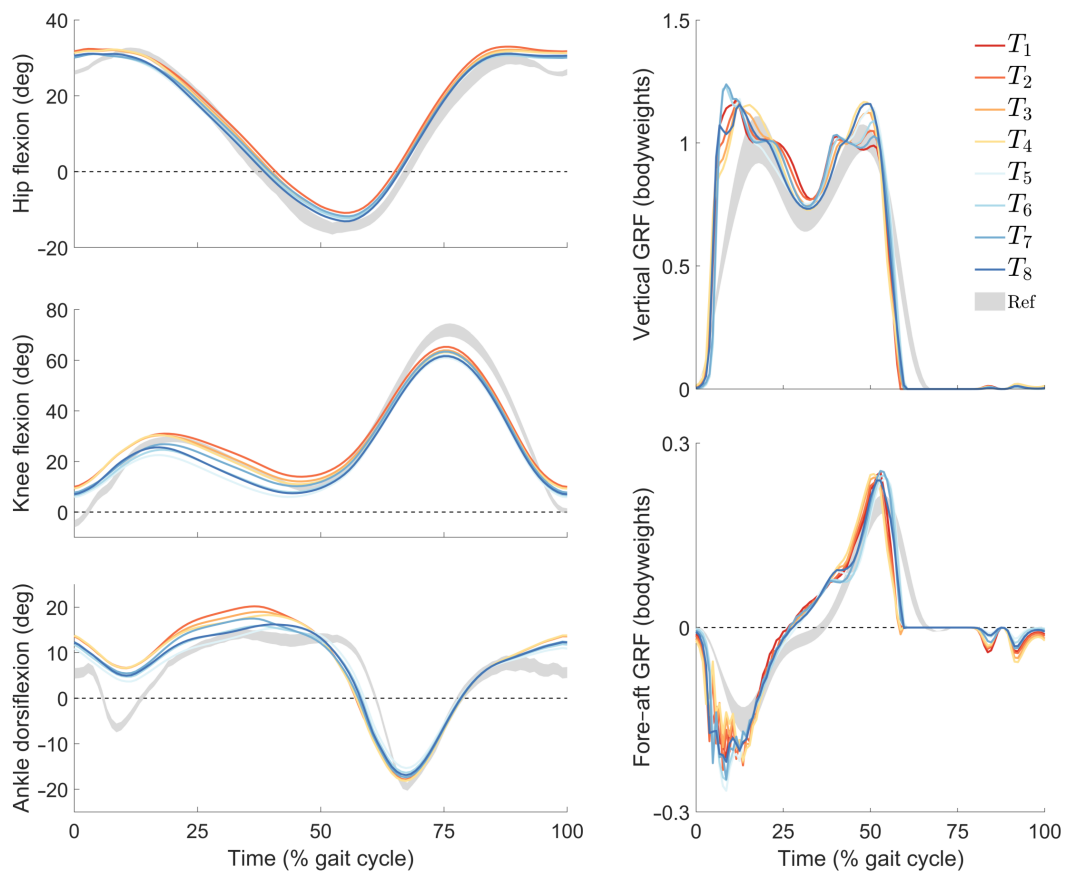


**Figure 2.** Joint kinematics and ground reaction forces from tracking simulations using cost functions  $T_1$  to  $T_8$ . (**Left**) Trajectories of the hip, knee, and ankle joints in the sagittal plane; (**right**) components of the ground reaction force (GRF) in the vertical and fore–aft directions. For reference, shaded regions (“Ref”) indicate gait patterns within one standard deviation of the mean from a population of healthy adults walking without assistance at similar speeds [35].

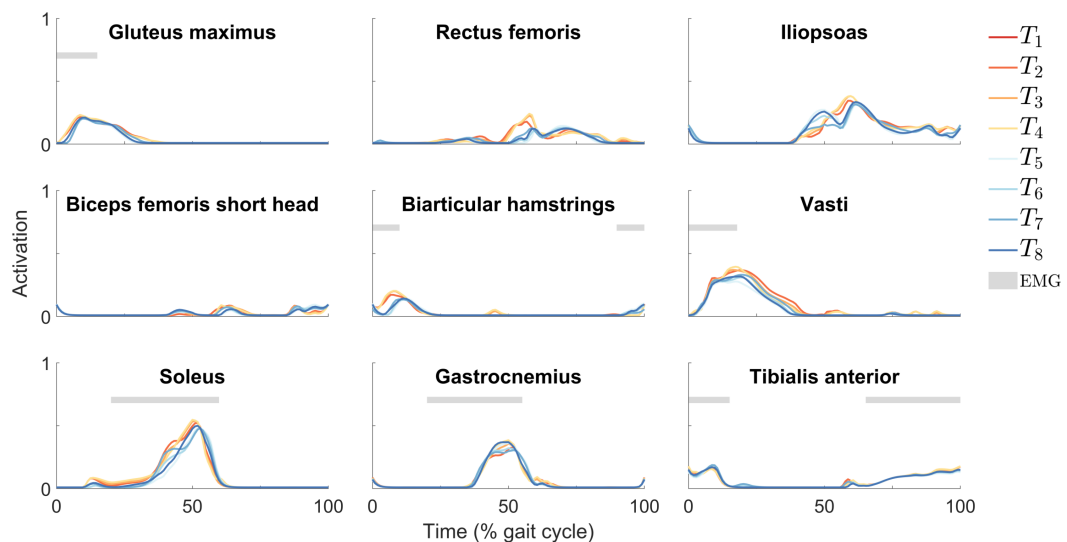


**Figure 3.** Muscle activations from tracking simulations using cost functions  $T_1$  to  $T_8$ . (**Left**) Uniarticular muscles on the posterior side of the leg; (**center**) biarticular muscles; (**right**) uniarticular muscles on the anterior side of the leg. For reference, horizontal bars (“EMG”) indicate periods of muscle activity from EMG data of healthy walking (no data were available for the rectus femoris, iliopsoas, or biceps femoris short head) [19].

**Table 3.** Each component of each cost function used in the tracking problem, evaluated at the obtained solution. Normalized values (in parentheses) have been multiplied by the normalization factor provided in Table 1. All optimizations converged to the specified tolerance. (GRF = ground reaction force.)

Cost Function	Component Value (Normalized)				
	State Tracking	GRF Tracking	Control Effort	Metabolic Energy	Head Acceleration
$T_1$	17.25 (1.15)	49.00 (0.95)	1.89 (0.96)	—	1.74 (0.97)
$T_2$	15.21 (1.02)	43.21 (0.83)	2.18 (1.10)	—	2.00 (1.11)
$T_3$	20.12 (1.34)	57.15 (1.10)	1.77 (0.90)	—	1.63 (0.91)
$T_4$	19.89 (1.33)	56.47 (1.09)	2.24 (1.14)	—	2.06 (1.15)
$T_5$	18.22 (1.22)	51.75 (1.00)	1.55 (0.79)	3.69 (0.95)	1.43 (0.79)
$T_6$	21.03 (1.40)	59.71 (1.15)	1.88 (0.96)	3.74 (0.96)	1.73 (0.96)
$T_7$	20.00 (1.34)	56.81 (1.10)	1.26 (0.64)	3.87 (0.99)	1.16 (0.64)
$T_8$	22.75 (1.52)	64.60 (1.25)	2.00 (1.01)	4.00 (1.03)	1.84 (1.02)

The joint kinematics and ground reaction forces for the predictive simulations of unassisted gait are shown in Figure 4. The most substantial difference between the predictive simulation results and the data measured from a population of healthy adults is that the knee flexion angle remains relatively constant during mid- to late stance, which contributes to producing a relatively flat vertical ground reaction force profile during stance. The knee is also slightly flexed at heel strike. Similar knee kinematics and ground reaction forces have been reported in other recent predictive simulations of gait [29,30,35]. With the exception of the results using cost function  $P_6$ , we note very similar results among all predictive simulations despite having been generated using different cost functions. In a computational study seeking to predict the relative effectiveness of various assistive devices, any one of these solutions could conceivably be selected as the “baseline” simulation against which each hypothetical assistance condition would be compared. The value of each cost function at the obtained solution and the corresponding cost of transport are provided in Table 4. The cost of transport varies from 3.39 J/kg/m (using cost function  $P_2$ ) to 5.08 J/kg/m (using  $P_3$ ).

**Table 4.** Each component of each cost function used to generate predictive simulations of unassisted gait, evaluated at the obtained solution, and the corresponding cost of transport. Normalized values (in parentheses) have been multiplied by the normalization factor provided in Table 2. All cost function values have been multiplied by 100 to improve clarity. All optimizations converged to the specified tolerance. (COT = cost of transport.)

Cost Function	Component Value (Normalized)				COT (J/kg/m)
	Control Effort	Metabolic Energy	Head Acceleration	Knee Load	
$P_1$	3.98 (2.02)	—	5.99 (3.33)	—	3.99
$P_2$	—	25.84 (6.63)	5.70 (3.16)	—	3.39
$P_3$	6.56 (3.33)	—	7.00 (3.89)	—	5.08
$P_4$	7.82 (3.97)	12.45 (3.19)	3.88 (2.16)	—	4.69
$P_5$	3.99 (2.03)	21.48 (5.51)	2.86 (1.59)	—	4.10
$P_6$	4.72 (2.40)	—	3.34 (1.86)	5.90 (0.01)	4.88

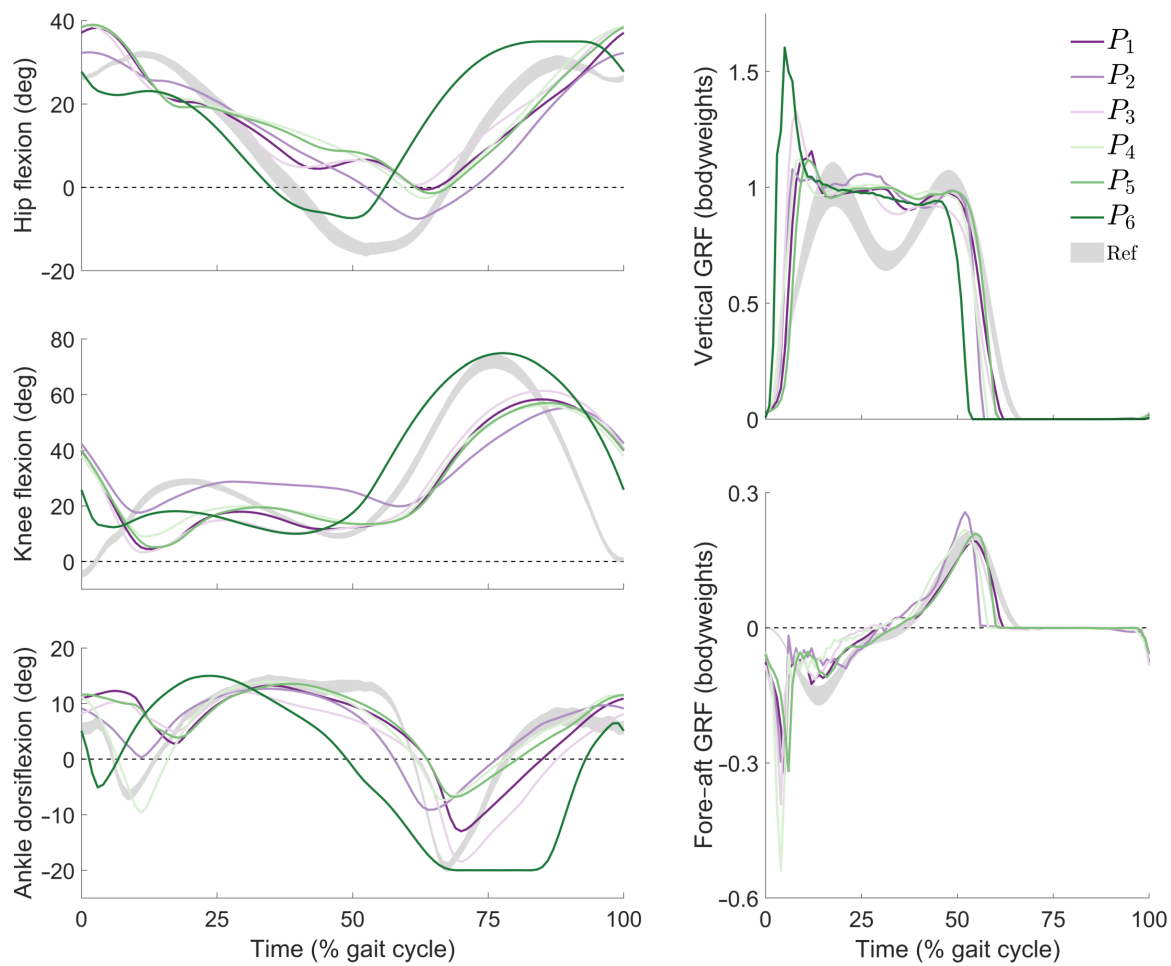


**Figure 4.** Joint kinematics and ground reaction forces from predictive simulations of unassisted gait using cost functions  $P_1$  to  $P_6$ . (Left) Trajectories of the hip, knee, and ankle joints in the sagittal plane; (right) components of the ground reaction force (GRF) in the vertical and fore-aft directions. For clarity, the fore-aft GRF component for  $P_6$  is not shown. For reference, shaded regions (“Ref”) indicate gait patterns within one standard deviation of the mean from a population of healthy adults walking without assistance at similar speeds [35].

The joint kinematics and ground reaction forces for the predictive simulations of device-assisted gait are shown in Figure 5 for hip flexion assistance, in Figure 6 for knee flexion assistance, and in Figure 7 for ankle plantarflexion assistance. Changes in joint kinematics were predicted when the devices were present, with the magnitude of the changes depending on both the assistance strategy and the cost function. With hip flexion assistance, all simulations predicted a relatively constant knee joint angle throughout stance and a shorter stance phase than typical unassisted gait. Knee flexion assistance had the effect of increasing the knee flexion angle during stance, decreasing the ankle dorsiflexion angle during midstance, and reducing the stance phase duration. Ankle plantarflexion assistance generally increased the ankle dorsiflexion angle throughout the gait cycle.

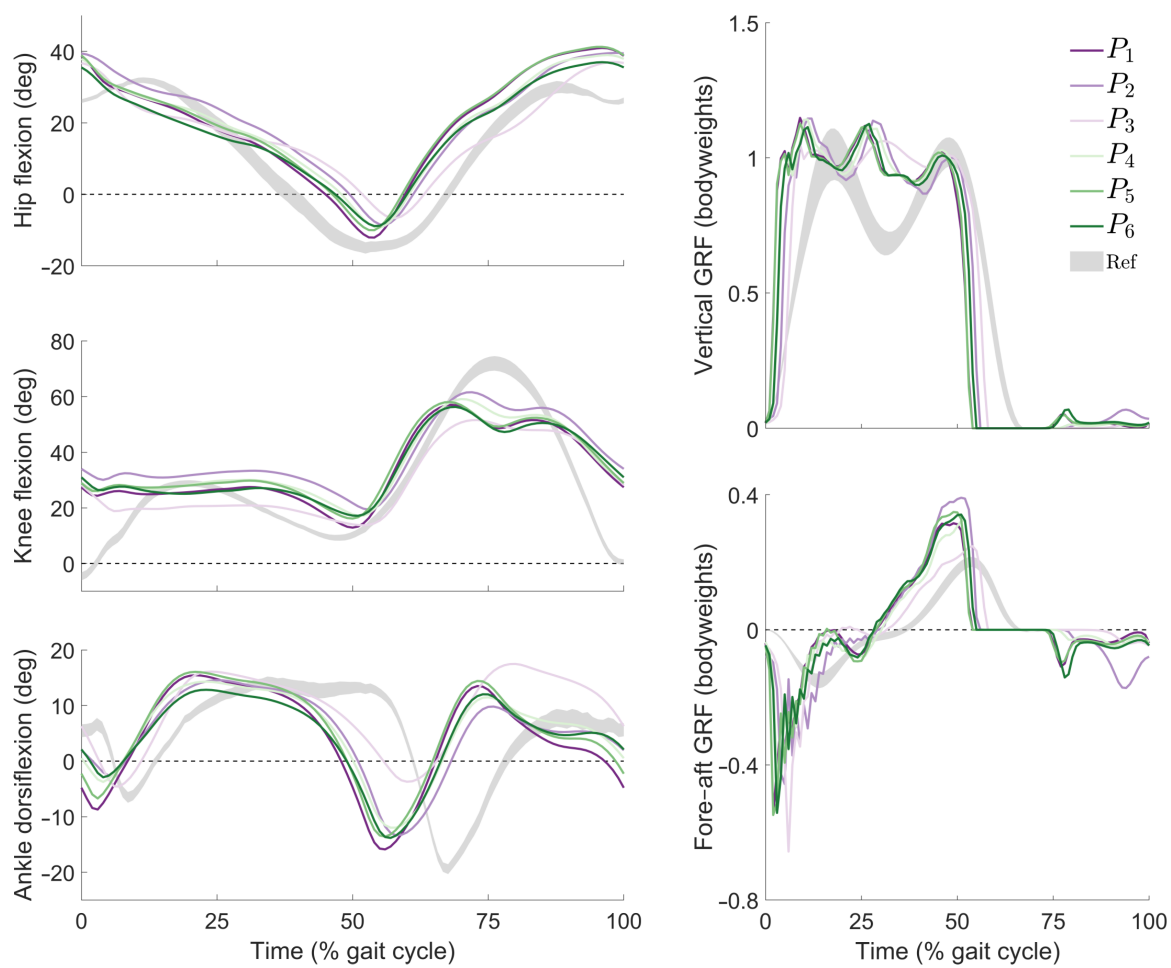


**Figure 5.** Joint kinematics and ground reaction forces from predictive simulations of gait with **hip flexion** assistance using cost functions  $P_1$  to  $P_6$ . (**Left**) Trajectories of the hip, knee, and ankle joints in the sagittal plane; (**right**) components of the ground reaction force (GRF) in the vertical and fore-aft directions. For reference, shaded regions (“Ref”) indicate gait patterns within one standard deviation of the mean from a population of healthy adults walking without assistance at similar speeds [35].

Although the joint kinematics were relatively insensitive to the cost function, the torques generated by the assistive devices varied substantially among cost functions, as shown in Figure 8. For example, with the exception of cost function  $P_3$ , all predictive simulations with hip flexion assistance had very similar joint trajectories (left column in Figure 5); however, the predicted device torques were dramatically different (Figure 8, top). The differences among the solutions predicted by different cost functions are further examined in Table 5. The predicted reduction in the cost of transport varied from 0.18 to 0.85 J/kg/m in absolute value, or from 5.4% to 17.4% of the cost of transport for the corresponding unassisted simulation. Peak assistive torques varied from 41.3 to 79.0 N·m and peak positive power varied from 143.1 to 299.6 W, which could lead to substantially different design requirements if predictive simulations are used to estimate specifications for physical components.

Similar results were observed with knee flexion assistance and ankle plantarflexion assistance, as shown in Tables 6 and 7, respectively. With knee flexion assistance, the predicted reduction in the cost of transport varied from 0.13 to 0.75 J/kg/m in absolute value, or from 3.8% to 15.3% of the cost of transport for the corresponding unassisted simulation; peak assistive torques varied from 48.0 to 94.2 N·m and peak positive power varied from 74.7 to 355.6 W. With ankle plantarflexion assistance, the predicted reduction in the cost of transport varied from 0.14 to 0.69 J/kg/m in absolute value, or from 3.4% to 14.2% of the cost of transport for the corresponding unassisted simulation; peak assistive

torques varied from 42.6 to 79.8 N·m and peak positive power varied from 67.5 to 124.2 W. Despite these differences, we note that all cost functions except  $P_2$  predicted the largest savings in the cost of transport with hip flexion assistance and the smallest savings with ankle plantarflexion assistance. These trends agree with the results of Dembia et al. [3] and reinforce the recommendation to explore devices that assist hip flexion if one is seeking to reduce the cost of transport.

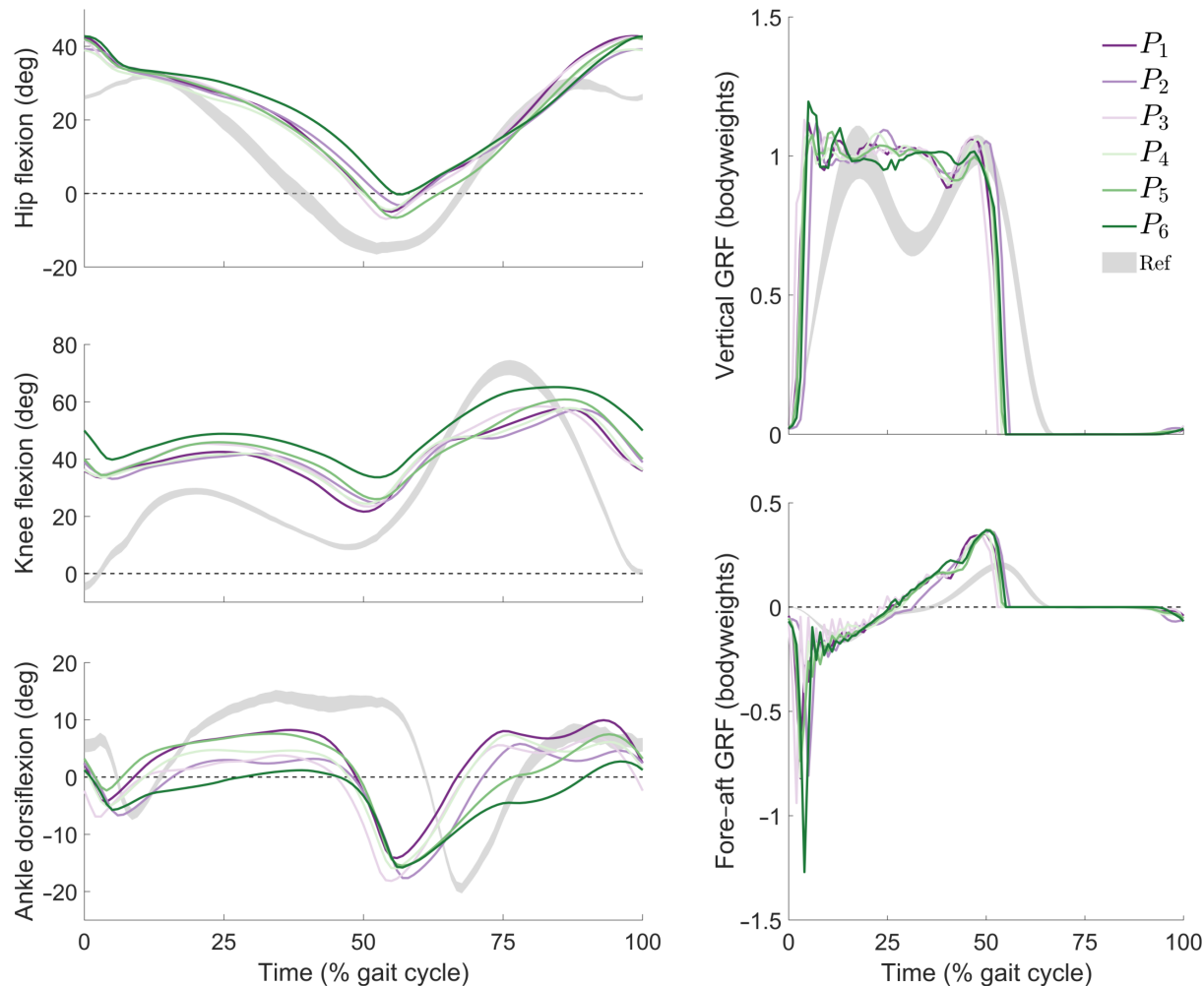


**Figure 6.** Joint kinematics and ground reaction forces from predictive simulations of gait with **knee flexion** assistance using cost functions  $P_1$  to  $P_6$ . **(Left)** Trajectories of the hip, knee, and ankle joints in the sagittal plane; **(right)** components of the ground reaction force (GRF) in the vertical and fore-aft directions. For reference, shaded regions (“Ref”) indicate gait patterns within one standard deviation of the mean from a population of healthy adults walking without assistance at similar speeds [35].

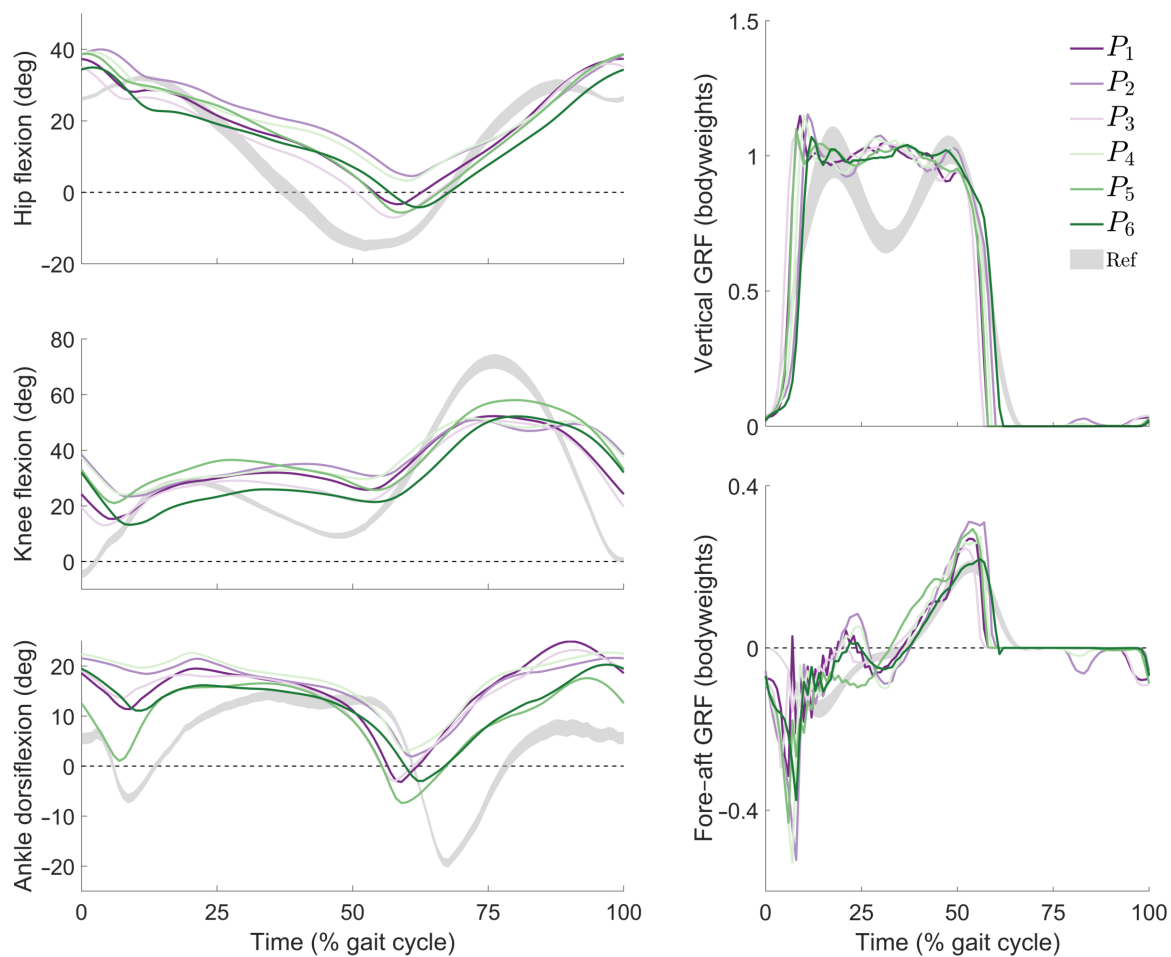


**Figure 7.** Joint kinematics and ground reaction forces from predictive simulations of gait with **ankle plantarflexion** assistance using cost functions  $P_1$  to  $P_6$ . (**Left**) Trajectories of the hip, knee, and ankle joints in the sagittal plane; (**right**) components of the ground reaction force (GRF) in the vertical and fore-aft directions. For reference, shaded regions (“Ref”) indicate gait patterns within one standard deviation of the mean from a population of healthy adults walking without assistance at similar speeds [35].

**Table 5.** Each component of each cost function used to generate predictive simulations of device-assisted gait with **hip flexion** assistance, evaluated at the obtained solution, and the corresponding cost of transport. Normalized values (in parentheses) have been multiplied by the normalization factor provided in Table 2. All cost function values have been multiplied by 100 to improve clarity. Percentage savings in the cost of transport are calculated relative to the cost of transport for the corresponding unassisted simulation. All optimizations converged to the specified tolerance.

Cost Function	Component Value (Normalized)				Cost of Transport	
	Control Effort	Metabolic Energy	Head Accel.	Knee Load	Value (J/kg/m)	Savings (%)
$P_1$	3.88 (1.97)	—	4.38 (2.43)	—	3.74	6.2
$P_2$	—	24.25 (6.22)	6.13 (3.40)	—	3.20	5.4
$P_3$	6.13 (3.11)	—	2.63 (1.46)	—	4.56	10.4
$P_4$	7.35 (3.73)	13.03 (3.34)	8.30 (4.61)	—	4.20	10.4
$P_5$	3.89 (1.97)	19.82 (5.08)	6.31 (3.51)	—	3.42	16.6
$P_6$	4.41 (2.24)	—	6.18 (3.43)	5.93 (0.01)	4.03	17.4

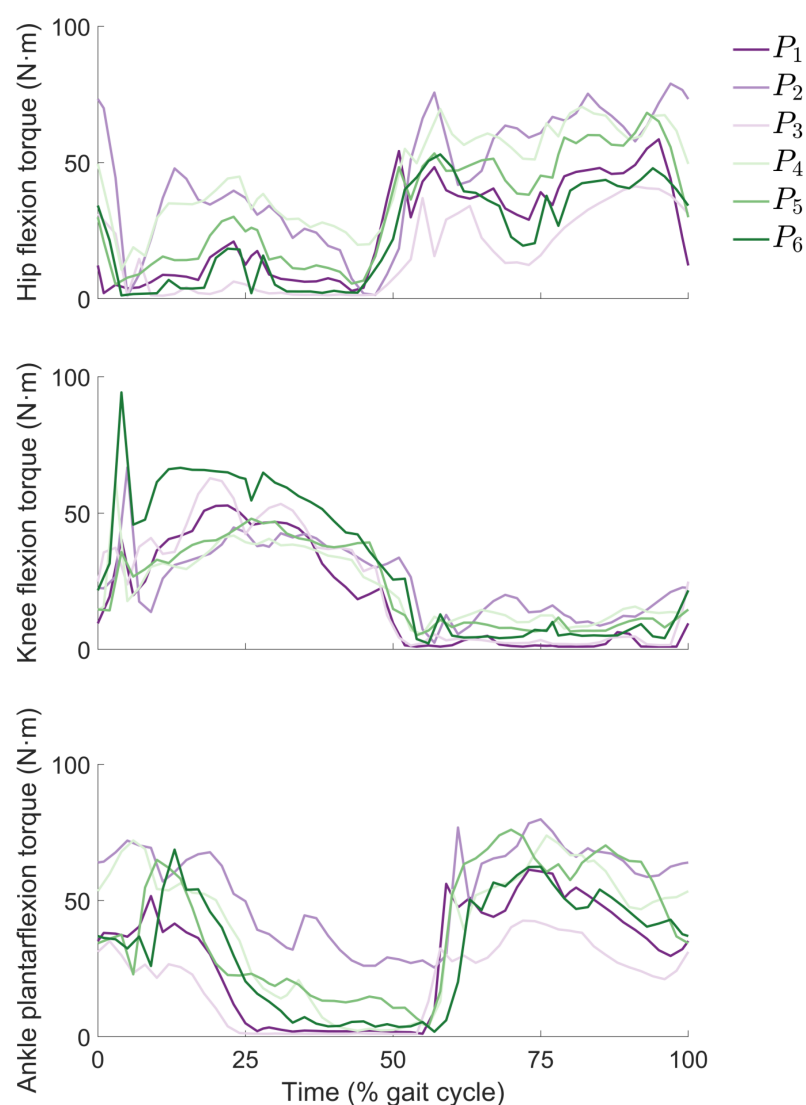


**Figure 8.** Device torques from predictive simulations of gait using cost functions  $P_1$  to  $P_6$ . (**Top**) Hip flexion assistance; (**center**) knee flexion assistance; (**bottom**) ankle plantarflexion assistance.

**Table 6.** Each component of each cost function used to generate predictive simulations of device-assisted gait with **knee flexion** assistance, evaluated at the obtained solution, and the corresponding cost of transport. Normalized values (in parentheses) have been multiplied by the normalization factor provided in Table 2. All cost function values have been multiplied by 100 to improve clarity. Percentage savings in the cost of transport are calculated relative to the cost of transport for the corresponding unassisted simulation. All optimizations converged to the specified tolerance.

Cost Function	Component Value (Normalized)					Cost of Transport	
	Control Effort	Metabolic Energy	Head Accel.	Knee Load	Value (J/kg/m)	Savings (%)	
$P_1$	4.16 (2.11)	—	4.14 (2.30)	—	3.81	4.4	
$P_2$	—	25.88 (6.64)	5.82 (3.23)	—	3.26	3.8	
$P_3$	5.82 (2.95)	—	2.51 (1.40)	—	4.68	8.0	
$P_4$	6.73 (3.42)	14.13 (3.62)	6.41 (3.56)	—	4.33	7.7	
$P_5$	3.66 (1.86)	18.59 (4.77)	5.13 (2.85)	—	3.54	13.7	
$P_6$	3.13 (1.59)	—	5.12 (2.85)	5.97 (0.02)	4.13	15.3	

**Table 7.** Each component of each cost function used to generate predictive simulations of device-assisted gait with **ankle plantarflexion** assistance, evaluated at the obtained solution, and the corresponding cost of transport. Normalized values (in parentheses) have been multiplied by the normalization factor provided in Table 2. All cost function values have been multiplied by 100 to improve clarity. Percentage savings in the cost of transport are calculated relative to the cost of transport for the corresponding unassisted simulation. All optimizations converged to the specified tolerance.

Cost Function	Component Value (Normalized)				Cost of Transport	
	Control Effort	Metabolic Energy	Head Accel.	Knee Load	Value (J/kg/m)	Savings (%)
$P_1$	4.17 (2.12)	—	3.89 (2.16)	—	3.85	3.4
$P_2$	—	22.56 (5.78)	5.83 (3.24)	—	3.13	7.6
$P_3$	5.12 (2.60)	—	2.96 (1.64)	—	4.72	7.3
$P_4$	6.33 (3.21)	11.48 (2.94)	6.64 (3.69)	—	4.40	6.2
$P_5$	2.57 (1.30)	19.66 (5.04)	4.20 (2.33)	—	3.56	13.2
$P_6$	2.33 (1.18)	—	7.25 (4.03)	5.98 (0.02)	4.19	14.2

#### 4. Conclusions

In this paper, we explored the potential of using predictive simulations to design assistive devices. Simulation-guided design offers many benefits, such as reducing the need to build physical prototypes and conduct time-consuming experiments, and allows device designers to focus their resources on comparing and optimizing only the most promising designs. Although predictive simulations are not expected to capture all phenomena that would be observed experimentally, one must consider the reliability of predictive simulations when applied to assistive device design—particularly if simulations are being used to predict absolute quantities (e.g., the cost of transport or peak motor torque) and not merely to compare the relative performance of different assistance strategies. We generated predictive simulations of walking in OpenSim Moco using a planar, bilaterally symmetric musculoskeletal model with 18 muscles. The musculoskeletal model was assumed to walk with a bilaterally symmetric gait to improve computational efficiency, as this permitted the simulation of only half of a gait cycle. Predictive simulations of unassisted walking were generated using six plausible cost functions, each of which produced a realistic gait pattern that could reasonably be used as the “baseline” simulation against which various assistance scenarios would be compared. The musculoskeletal model was then augmented with motors that generated hip flexion, knee flexion, or ankle plantarflexion torques, and the torques generated by the assistive devices were optimized along with the muscle forces and the motion of the model.

Although the cost functions that we explored produced predictive simulations with similar joint kinematics, the predicted savings in the cost of transport and the predicted torques and powers of the assistive devices were dramatically different. Depending on the cost function that was used, one could estimate metabolic savings of 5.4–17.4% with hip flexion assistance, 3.8–15.3% with knee flexion assistance, and 3.4–14.2% with ankle plantarflexion assistance. Broad ranges were also observed in peak assistive device torques: 41.3–79.0 N·m for the hip flexion actuators, 48.0–94.2 N·m for the knee flexion actuators, and 42.6–79.8 N·m for the ankle plantarflexion actuators. These differences could lead to substantially different design requirements when selecting actuators, batteries, and supporting hardware.

Two important limitations should be noted regarding the generalizability of our results. First, we used a simplified musculoskeletal model with 18 muscles and studied its motion in only the sagittal plane. This modeling strategy was chosen to ensure that the computational effort required to generate the predictive simulations remained relatively low; however, non-sagittal-plane motions and the muscle activity responsible for generating these motions were ignored. A more detailed model would be required to study phenomena such as motion in the frontal plane and selective weakness of muscles that were not

included in this model. Second, the model was bilaterally symmetric, assistive devices were added to both legs, and bilateral symmetry was enforced in the model's kinematics. The assumption of symmetry permitted the simulation of only half of a gait cycle, again to reduce computational effort, but this assumption limits the generalizability of the results. A modeling and simulation strategy that permits asymmetry would be required to study assistive technologies for individuals with hemiplegia and other conditions that result in substantial asymmetry.

This study highlights the importance of evaluating the sensitivity of predictive simulations to the cost function and weights that are selected. The absolute values of quantities of interest were observed to be sensitive to the selected cost function; however, comparisons between conditions when using a fixed cost function were relatively robust. All cost functions except for  $P_2$  predicted the largest reductions in the cost of transport with hip flexion assistance and the smallest reductions with ankle plantarflexion assistance. To generalize these results, the analysis should be repeated to study walking under different conditions (e.g., at different speeds, on slopes, and during load carriage), running at a range of speeds, and using different musculoskeletal models. Different terms in the cost function could be explored as well, including penalties for large time derivatives of ground reaction forces, penalties for large passive joint torques generated by ligaments, and penalties for features of gait that would cause instability, as these factors may contribute to shaping the gait patterns observed in nature. Experimental validation over a large population moving in a large range of scenarios would build confidence in the predictive capability of a given cost function when used with a given musculoskeletal model.

**Author Contributions:** Conceptualization, T.K.U.; Data curation, A.N.; Formal analysis, A.N. and T.K.U.; Funding acquisition, T.K.U.; Investigation, A.N.; Methodology, A.N. and T.K.U.; Project administration, T.K.U.; Resources, A.N. and T.K.U.; Software, A.N.; Supervision, T.K.U.; Validation, A.N. and T.K.U.; Visualization, A.N. and T.K.U.; Writing—original draft, A.N. and T.K.U.; Writing—review and editing, A.N. and T.K.U. All authors have read and agreed to the published version of the manuscript.

**Funding:** This work was supported by the Natural Sciences and Engineering Research Council of Canada (RGPIN-2019-05726 [T.K.U.]). The funders had no role in the study design, data collection and analysis, decision to publish, or preparation of the manuscript.

**Data Availability Statement:** We performed this study using the OpenSim Moco software, which is open source and freely available at <https://simtk.org/projects/opensim>, (accessed on 19 October 2022). The data presented in this study are openly available at [https://simtk.org/projects/cost\\_fn\\_snstvty](https://simtk.org/projects/cost_fn_snstvty), (accessed on 19 October 2022).

**Acknowledgments:** The authors thank Carmichael Ong for his technical support, and the developers of OpenSim Moco for making this tool freely available to the community.

**Conflicts of Interest:** The authors declare no conflict of interest.

## References

1. Farris, D.J.; Sawicki, G.S. The mechanics and energetics of human walking and running: A joint level perspective. *J. R. Soc. Interface* **2012**, *9*, 110–118. [[CrossRef](#)]
2. Umberger, B.R. Stance and swing phase costs in human walking. *J. R. Soc. Interface* **2010**, *7*, 1329–1340. [[CrossRef](#)] [[PubMed](#)]
3. Dembia, C.L.; Silder, A.; Uchida, T.K.; Hicks, J.L.; Delp, S.L. Simulating ideal assistive devices to reduce the metabolic cost of walking with heavy loads. *PLoS ONE* **2017**, *12*, e0180320. [[CrossRef](#)] [[PubMed](#)]
4. Uchida, T.K.; Hicks, J.L.; Dembia, C.L.; Delp, S.L. Stretching your energetic budget: how tendon compliance affects the metabolic cost of running. *PLoS ONE* **2016**, *11*, e0150378. [[CrossRef](#)] [[PubMed](#)]
5. Al Borno, M.; Hicks, J.L.; Delp, S.L. The effects of motor modularity on performance, learning and generalizability in upper-extremity reaching: a computational analysis. *J. R. Soc. Interface* **2020**, *17*, 20200011. [[CrossRef](#)]
6. Tigrini, A.; Verdini, F.; Fioretti, S.; Mengarelli, A. Center of pressure plausibility for the double-link human stance model under the intermittent control paradigm. *J. Biomech.* **2021**, *128*, 110725. [[CrossRef](#)]
7. Mehrabi, N.; Schwartz, M.H.; Steele, K.M. Can altered muscle synergies control unimpaired gait? *J. Biomech.* **2019**, *90*, 84–91. [[CrossRef](#)]

8. Uchida, T.K.; Delp, S.L. *Biomechanics of Movement: The Science of Sports, Robotics, and Rehabilitation*; MIT Press: Cambridge, MA, USA, 2021.
9. Arnold, E.M.; Hamner, S.R.; Seth, A.; Millard, M.; Delp, S.L. How muscle fiber lengths and velocities affect muscle force generation as humans walk and run at different speeds. *J. Exp. Biol.* **2013**, *216*, 2150–2160. [[CrossRef](#)]
10. Uchida, T.K.; Seth, A.; Pouya, S.; Dembia, C.L.; Hicks, J.L.; Delp, S.L. Simulating ideal assistive devices to reduce the metabolic cost of running. *PLoS ONE* **2016**, *11*, e0163417. [[CrossRef](#)]
11. Lee, G.; Kim, J.; Panizzolo, F.A.; Zhou, Y.M.; Baker, L.M.; Galiana, I.; Malcolm, P.; Walsh, C.J. Reducing the metabolic cost of running with a tethered soft exosuit. *Sci. Robot.* **2017**, *2*, eaan6708. [[CrossRef](#)]
12. Collins, S.H.; Wiggin, M.B.; Sawicki, G.S. Reducing the energy cost of human walking using an unpowered exoskeleton. *Nature* **2015**, *522*, 212–215. [[CrossRef](#)] [[PubMed](#)]
13. Sawicki, G.S.; Khan, N.S. A simple model to estimate plantarflexor muscle–tendon mechanics and energetics during walking with elastic ankle exoskeletons. *IEEE Trans. Biomed. Eng.* **2016**, *63*, 914–923. [[CrossRef](#)] [[PubMed](#)]
14. Gordon, K.E.; Ferris, D.P. Learning to walk with a robotic ankle exoskeleton. *J. Biomech.* **2007**, *40*, 2636–2644. [[CrossRef](#)] [[PubMed](#)]
15. Kao, P.C.; Lewis, C.L.; Ferris, D.P. Invariant ankle moment patterns when walking with and without a robotic ankle exoskeleton. *J. Biomech.* **2010**, *43*, 203–209. [[CrossRef](#)] [[PubMed](#)]
16. Galle, S.; Malcolm, P.; Derave, W.; De Clercq, D. Adaptation to walking with an exoskeleton that assists ankle extension. *Gait Posture* **2013**, *38*, 495–499. [[CrossRef](#)]
17. Lenzi, T.; Carrozza, M.C.; Agrawal, S.K. Powered hip exoskeletons can reduce the user’s hip and ankle muscle activations during walking. *IEEE Trans. Neural Syst. Rehabil. Eng.* **2013**, *21*, 938–948. [[CrossRef](#)]
18. Anderson, F.C.; Pandy, M.G. Dynamic optimization of human walking. *J. Biomech. Eng.* **2001**, *123*, 381–390. [[CrossRef](#)]
19. Dorn, T.W.; Wang, J.M.; Hicks, J.L.; Delp, S.L. Predictive simulation generates human adaptations during loaded and inclined walking. *PLoS ONE* **2015**, *10*, e0121407. [[CrossRef](#)]
20. Handford, M.L.; Srinivasan, M. Robotic lower limb prosthesis design through simultaneous computer optimizations of human and prosthesis costs. *Sci. Rep.* **2016**, *6*, 19983. [[CrossRef](#)]
21. Handford, M.L.; Srinivasan, M. Energy-optimal human walking with feedback-controlled robotic prostheses: A computational study. *IEEE Trans. Neural Syst. Rehabil. Eng.* **2018**, *26*, 1773–1782. [[CrossRef](#)]
22. Selinger, J.C.; O’Connor, S.M.; Wong, J.D.; Donelan, J.M. Humans can continuously optimize energetic cost during walking. *Curr. Biol.* **2015**, *25*, 2452–2456. [[CrossRef](#)] [[PubMed](#)]
23. Davy, D.T.; Audu, M.L. A dynamic optimization technique for predicting muscle forces in the swing phase of gait. *J. Biomech.* **1987**, *20*, 187–201. [[CrossRef](#)] [[PubMed](#)]
24. Miller, R.H.; Umberger, B.R.; Hamill, J.; Caldwell, G.E. Evaluation of the minimum energy hypothesis and other potential optimality criteria for human running. *Proc. R. Soc. Lond. B Biol. Sci.* **2012**, *279*, 1498–1505. [[CrossRef](#)] [[PubMed](#)]
25. Fey, N.P.; Klute, G.K.; Neptune, R.R. Optimization of prosthetic foot stiffness to reduce metabolic cost and intact knee loading during below-knee amputee walking: A theoretical study. *J. Biomech. Eng.* **2012**, *134*, 111005. [[CrossRef](#)] [[PubMed](#)]
26. Koelewijn, A.D.; Dorschky, E.; van den Bogert, A.J. A metabolic energy expenditure model with a continuous first derivative and its application to predictive simulations of gait. *Comput. Methods Biomed. Eng.* **2018**, *21*, 521–531. [[CrossRef](#)]
27. Lin, Y.C.; Walter, J.P.; Pandy, M.G. Predictive simulations of neuromuscular coordination and joint-contact loading in human gait. *Ann. Biomed. Eng.* **2018**, *46*, 1216–1227. [[CrossRef](#)]
28. Falisse, A.; Serrancolí, G.; Dembia, C.L.; Gillis, J.; Jonkers, I.; De Groote, F. Rapid predictive simulations with complex musculoskeletal models suggest that diverse healthy and pathological human gaits can emerge from similar control strategies. *J. R. Soc. Interface* **2019**, *16*, 20190402. [[CrossRef](#)] [[PubMed](#)]
29. Ong, C.F.; Geijtenbeek, T.; Hicks, J.L.; Delp, S.L. Predicting gait adaptations due to ankle plantarflexor muscle weakness and contracture using physics-based musculoskeletal simulations. *PLoS Comput. Biol.* **2019**, *15*, e1006993. [[CrossRef](#)]
30. Veerkamp, K.; Waterval, N.F.J.; Geijtenbeek, T.; Carty, C.P.; Lloyd, D.G.; Harlaar, J.; van der Krogt, M.M. Evaluating cost function criteria in predicting healthy gait. *J. Biomech.* **2021**, *123*, 110530. [[CrossRef](#)]
31. Kaplan, M.L.; Heegaard, J.H. Predictive algorithms for neuromuscular control of human locomotion. *J. Biomech.* **2001**, *34*, 1077–1083. [[CrossRef](#)]
32. Srinivasan, M. Fifteen observations on the structure of energy-minimizing gaits in many simple biped models. *J. R. Soc. Interface* **2011**, *8*, 74–98. [[CrossRef](#)] [[PubMed](#)]
33. Rebula, J.R.; Kuo, A.D. The cost of leg forces in bipedal locomotion: A simple optimization study. *PLoS ONE* **2015**, *10*, e0117384. [[CrossRef](#)] [[PubMed](#)]
34. Koelewijn, A.D.; van den Bogert, A.J. Joint contact forces can be reduced by improving joint moment symmetry in below-knee amputee gait simulations. *Gait Posture* **2016**, *49*, 219–225. [[CrossRef](#)] [[PubMed](#)]
35. Falisse, A.; Serrancolí, G.; Dembia, C.L.; Gillis, J.; De Groote, F. Algorithmic differentiation improves the computational efficiency of OpenSim-based trajectory optimization of human movement. *PLoS ONE* **2019**, *14*, e0217730. [[CrossRef](#)] [[PubMed](#)]
36. McDonald, K.A.; Cusumano, J.P.; Hieronymi, A.; Rubenson, J. Humans trade off whole-body energy cost to avoid overburdening muscles while walking. *Proc. R. Soc. Lond. B Biol. Sci.* **2022**, *289*, 20221189. [[CrossRef](#)] [[PubMed](#)]
37. Koelewijn, A.D.; Selinger, J.C. Predictive simulations to replicate human gait adaptations and energetics with exoskeletons. *IEEE Trans. Neural Syst. Rehabil. Eng.* **2022**, *30*, 1931–1940. [[CrossRef](#)]

38. Ackermann, M.; van den Bogert, A.J. Optimality principles for model-based prediction of human gait. *J. Biomech.* **2010**, *43*, 1055–1060. [[CrossRef](#)]
39. Xiang, Y.; Arora, J.S.; Abdel-Malek, K. Optimization-based prediction of asymmetric human gait. *J. Biomech.* **2011**, *44*, 683–693. [[CrossRef](#)]
40. Dembia, C.L.; Bianco, N.A.; Falisse, A.; Hicks, J.L.; Delp, S.L. OpenSim Moco: musculoskeletal optimal control. *PLoS Comput. Biol.* **2020**, *16*, e1008493. [[CrossRef](#)]
41. Park, S.; Caldwell, G.E.; Umberger, B.R. A direct collocation framework for optimal control simulation of pedaling using OpenSim. *PLoS ONE* **2022**, *17*, e0264346. [[CrossRef](#)]
42. Gupta, D.; Donnelly, C.J.; Reinbolt, J.A. Optimizing whole-body kinematics using OpenSim Moco to reduce peak non-sagittal plane knee loads and ACL injury risk during single leg jump landing. In Proceedings of the Virtual 44th Meeting of the American Society of Biomechanics, Atlanta, GA, USA, 4–7 August 2020; p. 129.
43. Ede, C.; Blenkinsop, G.; Allen, S. Estimating the variability of hamstring function with increasing running speed using direct collocation. *ISBS Proc. Arch.* **2022**, *40*, 40.
44. Fox, A.S.; Bonacci, J.; Gill, S.D.; Page, R.S. Simulating the effect of glenohumeral capsulorrhaphy on kinematics and muscle function. *J. Orthop. Res.* **2021**, *39*, 880–890. [[CrossRef](#)] [[PubMed](#)]
45. Delp, S.L.; Anderson, F.C.; Arnold, A.S.; Loan, P.; Habib, A.; John, C.T.; Guendelman, E.; Thelen, D.G. OpenSim: open-source software to create and analyze dynamic simulations of movement. *IEEE Trans. Biomed. Eng.* **2007**, *54*, 1940–1950. [[CrossRef](#)] [[PubMed](#)]
46. Seth, A.; Hicks, J.L.; Uchida, T.K.; Habib, A.; Dembia, C.L.; Dunne, J.J.; Ong, C.F.; DeMers, M.S.; Rajagopal, A.; Millard, M.; et al. OpenSim: Simulating musculoskeletal dynamics and neuromuscular control to study human and animal movement. *PLoS Comput. Biol.* **2018**, *14*, e1006223. [[CrossRef](#)]
47. De Groote, F.; Kinney, A.L.; Rao, A.V.; Fregly, B.J. Evaluation of direct collocation optimal control problem formulations for solving the muscle redundancy problem. *Ann. Biomed. Eng.* **2016**, *44*, 2922–2936. [[CrossRef](#)]
48. Serrancolí, G.; Falisse, A.; Dembia, C.; Vantilt, J.; Tanghe, K.; Lefeber, D.; Jonkers, I.; De Schutter, J.; De Groote, F. Subject-exoskeleton contact model calibration leads to accurate interaction force predictions. *IEEE Trans. Neural Syst. Rehabil. Eng.* **2019**, *27*, 1597–1605. [[CrossRef](#)]
49. Hunt, K.H.; Crossley, F.R.E. Coefficient of restitution interpreted as damping in vibroimpact. *J. Appl. Mech.* **1975**, *42*, 440–445. [[CrossRef](#)]
50. Lin, Y.C.; Pandy, M.G. Three-dimensional data-tracking dynamic optimization simulations of human locomotion generated by direct collocation. *J. Biomech.* **2017**, *59*, 1–8. [[CrossRef](#)]
51. Bhargava, L.J.; Pandy, M.G.; Anderson, F.C. A phenomenological model for estimating metabolic energy consumption in muscle contraction. *J. Biomech.* **2004**, *37*, 81–88. [[CrossRef](#)]
52. Nguyen, V.Q.; Johnson, R.T.; Sup, F.C.; Umberger, B.R. Bilevel optimization for cost function determination in dynamic simulation of human gait. *IEEE Trans. Neural Syst. Rehabil. Eng.* **2019**, *27*, 1426–1435. [[CrossRef](#)]